Superconductivity and topological properties of MgB_2-type diborides from first principles

Yipeng An,[1,*] Jie Li,[2] Kun Wang,[3,4] Guangtao Wang,[1] Shijing Gong,[5] Chunlan Ma,[6] Tianxing Wang,[1] Zhaoyong Jiao,[1] Xiao Dong,[1] Guoliang Xu,[1] Ruqian Wu,[2,†] and Wuming Liu[7,‡]

[1]*School of Physics, Henan Normal University, Xinxiang 453007, China*

[2]*Department of Physics and Astronomy, University of California, Irvine, California 92697, USA*

[3]*Department of Physics and Astronomy, Mississippi State University, Starkville, Mississippi 39762, USA*

[4]*Department of Chemistry, Mississippi State University, Starkville, Mississippi 39762, USA*

[5]*Key Laboratory of Polar Materials and Devices (MOE) & Department of Optoelectronics, East China Normal University, Shanghai 200062, China*

[6]*School of Physics and Technology, Suzhou University of Science and Technology, Suzhou 215009, China*

[7]*Beijing National Laboratory for Condensed Matter Physics, Institute of Physics, Chinese Academy of Sciences, Beijing 100190, China*

(Received 9 June 2021; revised 23 September 2021; accepted 24 September 2021; published 14 October 2021)

The superconductivities and topological properties of MgB_2-type diborides are investigated by means of first-principles calculations with different exchange-correlation functionals. Functionals with the van der Waals (vdW) correction (such as OptB88-vdW) may predict critical temperature (T_c) comparable with experimental results for several MgB_2-type superconductors, particularly for the pristine MgB_2 (39.3 vs 39 K). Interestingly, the spin-fluctuation is found to play a significant role in the superconducting behavior of diborides with transition metal elements, and their T_c can be enhanced monotonically by applying tensile strains. Furthermore, Dirac surface states of TaB_2 and NbB_2 are revealed, suggesting their potential use as topological superconducting materials. This paper provides a useful guideline for *ab initio* studies of superconductivities and topological properties of vdW layered materials.

DOI: 10.1103/PhysRevB.104.134510

I. INTRODUCTION

To search and design superconductors for applications, one of the sensible strategies is predicting their critical temperature (T_c) from ground state properties at zero temperature with a dependable theoretical framework. Although it remains a challenge to achieve this goal for general superconducting materials, a few successful theories have been developed in the last half century, and the seminal theory of Bardeen, Cooper, and Schrieffer (BCS) was the outstanding example [1]. In principle, the anisotropic Migdal-Eliashberg (ME) approach [2,3] can provide reliable quantitative determination of anisotropic temperature-dependent superconducting gap (Δ) and T_c of conventional superconductors that rely on phonon-mediated interaction between electrons. The computational cost can be further reduced by combing with electron-phonon coupling (EPC) interpolation based on maximally localized Wannier functions [4–7]. Empirical models such as the Morel-Anderson theory [8] and McMillan's formula [9–11] using adjustable parameters may also give T_c of conventional isotropic superconductors close to the solution of the Eliashberg equations [12].

In recent years, the application of density functional theory (DFT) for studies of superconductors (SCDFT) was proved to be powerful in predicting new superconducting materials without the need for empirical parameters [13–15] as well as in explaining the physical mechanisms of superconductivity [16–19], especially for cases under pressure [20]. A great deal of effort has been dedicated to further empower the predictability of the SCDFT scheme by examining or developing appropriate exchange-correlation functionals [18], considering the anisotropic natures of EPC, or including plasmons [21], spin-fluctuation (SF) [22], and the spin-orbit interaction [23]. Particularly, as the complexities of many-body interactions are mostly invoked in the exchange and correlation term, the applicability of different functionals for the studies of superconductivity has not been carefully examined, and poor results were occasionally obtained. For instance, T_c of a prototypical anisotropic superconductor MgB_2 was reported to be only 22 K [24] via DFT calculations with the generalized gradient approximation (GGA) [25] and ultrasoft pseudopotentials [26], far smaller than its experiment value of 39 K [27]. This value was increased to 35.4 K by using a newly developed functional [18], showing a large room for getting accurate description of superconductivities with *ab initio* theory.

In this paper, we study the superconductivities of several MgB_2-type diborides with the van der Waals (vdW) layered structure, namely, MgB_2 and VB-group diborides MB_2 (M = V, Nb, Ta), by means of first-principles calculations. We evaluate different exchange-correlation functionals, from the conventional Perdew-Burke-Ernzerhof (PBE) functional [25,28], revPBE [29], PBEsol [30], to those with the vdW correction, such as OptB88-vdW (OPT) [31–33], which has

*ypan@htu.edu.cn
†wur@uci.edu
‡wmliu@iphy.ac.cn

been widely used for the structural optimization of vdW layered materials [34,35]. Our results unveil that the OPT functional can provide excellent results of superconductivities of MgB_2-type vdW layered structures, including giving the best theoretical $T_c = 39.3$ K of MgB_2 to date. Our other key results include (1) a reasonable stretch strain may lead to monotonical increase of T_c, (2) the spin fluctuation plays a significant role in determining the superconductivities of VB-group diborides, and (3) TaB_2 and NbB_2 show time-reversal symmetry-protected topological Dirac surface states in their spectral function. These findings open a vista for exploring emergent properties of superconducting and topological materials and, more importantly, for integrating them in potential applications.

II. COMPUTATIONAL DETAILS

According to the SCDFT, the critical superconducting gap at a wave vector $\mathbf{k}$ is described as

$$\Delta_{n\mathbf{k}} = -\frac{1}{2}\sum_{n'\mathbf{k}'} \frac{K_{n\mathbf{k}n'\mathbf{k}'}(\xi_{n\mathbf{k}}, \xi_{n'\mathbf{k}'})}{1 + Z_{n\mathbf{k}}(\xi_{n\mathbf{k}})} \frac{\Delta_{n'\mathbf{k}'}}{\sqrt{\xi^2_{n'\mathbf{k}'} + \Delta^2_{n'\mathbf{k}'}}} \times \tanh\left(\frac{\sqrt{\xi^2_{n'\mathbf{k}'} + \Delta^2_{n'\mathbf{k}'}}}{2T}\right), \quad (1)$$

where $\xi_{n\mathbf{k}}$ is the nth eigenvalue of the normal-state Kohn-Sham (KS) orbital measured from the Fermi level (E_F). Here, $K_{n\mathbf{k}n'\mathbf{k}'}(\xi, \xi')$ refers to the superconducting pair creation and annihilation interactions with the following three terms:

$$K_{n\mathbf{k}n'\mathbf{k}'}(\xi, \xi') \equiv K^{ee}_{n\mathbf{k}n'\mathbf{k}'}(\xi, \xi') + K^{\mathrm{ep}}_{n\mathbf{k}n'\mathbf{k}'}(\xi, \xi') + K^{\mathrm{sf}}_{n\mathbf{k}n'\mathbf{k}'}(\xi, \xi'), \quad (2)$$

namely, the electron-electron Coulomb repulsion, the EPC, and the alternative spin-fluctuation kernel. The electron-phonon renormalization factor $Z_{n\mathbf{k}}(\xi)$ is comprised of the EPC and alternative SF terms as

$$Z_{n\mathbf{k}}(\xi) = Z^{\mathrm{ep}}_{n\mathbf{k}}(\xi) + Z^{\mathrm{sf}}_{n\mathbf{k}}(\xi), \quad (3)$$

as the contribution from the Coulomb repulsion is already included in the KS eigenvalue $\xi_{n\mathbf{k}}$. Here, T is the temperature defined by considering the Boltzmann constant $k_B = 1$. More details about the forms of K and Z used in this paper can be found in previous reports [14,19]. Note that a recently proposed functional of K and Z sets a new standard for the balance of accuracy and computational cost in simulating the superconductivity [18]. The T_c is obtained using the bisection method [19], with the initial lower limit $T_c^{\min}$ being set to zero, and the initial upper limit $T_c^{\max}$ being set according to the BCS theory ($2\Delta_0/3.54$, where Δ_0 refers to the superconducting gap averaged over Fermi surfaces at 0 K, this value is doubled if there is a finite gap at this temperature). The gap Eq. (1) is solved at $T = (T_c^{\min} + T_c^{\max})/2$, and either $T_c^{\max}$ or $T_c^{\min}$ is replaced by T in the following steps based on whether the amplitude of average gap is small enough (i.e., $\langle|\Delta|\rangle < 10^{-3}\Delta_0$). The procedure repeats 10 times, and T_c is obtained as the average of $T_c^{\min}$ and $T_c^{\max}$, which are very close to each other.

In this paper, the first-principles self-consistent and EPC calculations are performed with the QUANTUMESPRESSO (QE) code [36]. The SG15 optimized norm-conserving Vanderbilt (ONCV) pseudopotentials [37–39] are employed to describe the effect of core electrons. The plane-wave kinetic energy cutoff and the energy cutoff for charge density are set to 80 and 320 Ry, respectively. Different exchange-correlation functionals are assessed [25,28–33]. The Brillouin-zone integrations are calculated by the optimized tetrahedron method [40] using a 12 × 12 × 12 grid. A denser grid (24 × 24 × 24) is used to obtain the density of states and band structures, while coarse grid (6 × 6 × 6) is adopted for the phonon calculations. The total energy tolerance and residual force on each atom are $<10^{-8}$ Ry and 10^{-6} Ry Bohr^{-1} in the geometry optimization. The phonon frequencies and electron-phonon vertices are obtained using density functional perturbation theory [41]. The SCDFT calculations are performed using the Superconducting-Toolkit (SCTK) [17,42]. The normal state of electronic structure is read from the self-consistent results of QE with the same k-points mesh. The EPC and kernel term of Eq. (2) are obtained with the same grid of k-points as in the phonon calculations.

The work function (Φ) and spectral function of surface structures are obtained by the surface Green's function method as implemented in the QUANTUMATK (ATK) [43–45]. Linear combinations of atomic orbitals are employed to expand the wave functions of valence states. The SG15 ONCV pseudopotentials [37–39], GGA-PBE functional [25,28], and

TABLE I. Superconducting parameters of MgB_2 with experimental structure[a] obtained with different functionals.

	PBE	revPBE	PBEsol	OptB88-vdW
T_c (K)[b]	23.4	24.0	19.3	39.3
$T_{c\text{-SF}}$ (K)	18.1	18.7	14.4	33.2
Z_{ave}	0.61	0.61	0.58	0.76
$\Delta_{\max}$ (meV)	5.99	6.02	5.22	9.63
$\Delta_{\min}$ (meV)	0.85	0.84	0.76	1.18
λ_{ave}	0.65	0.64	0.61	0.80
μ^*_{ave}	0.28	0.28	0.28	0.28

[a]The experimental structure with lattice **a** (**c**) = 3.086(3.524) Å [27].
[b]The experimental T_c is 39 K [27], and other theoretical T_c are 35.4 K [18], 34.1 K [50], and 49 K [4], respectively.

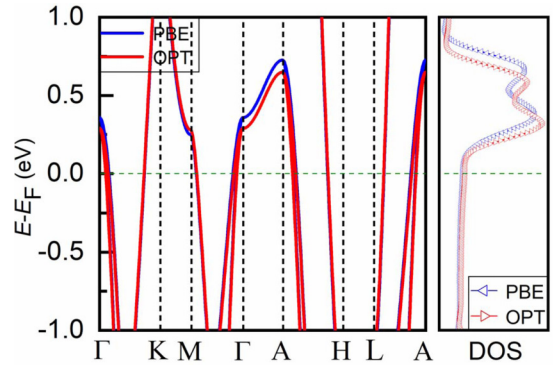

FIG. 1. Band structures and density of states (DOS) of MgB_2 obtained with PBE and OptB88-vdW (OPT) functionals, respectively. The E_F is shifted to zero.

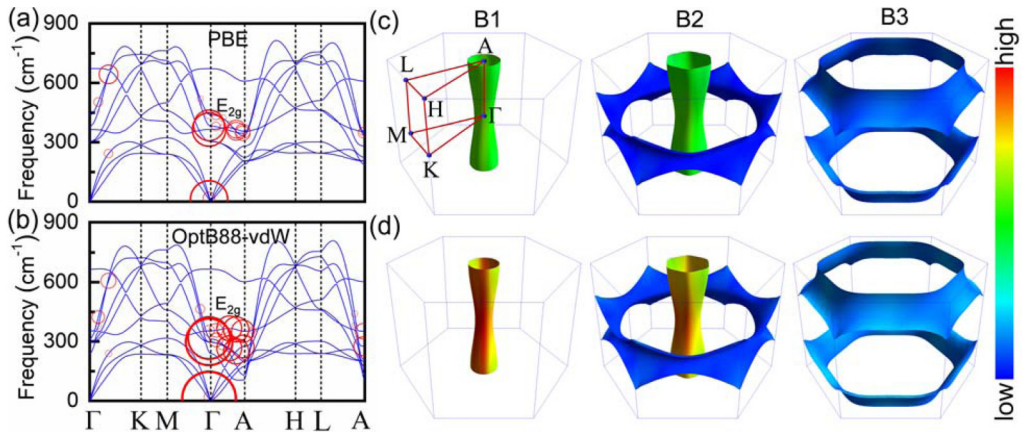

FIG. 2. Phonon band structures, electron-phonon coupling (EPC) constants $\lambda_{\mathbf{q}v}$, and $\lambda_{n\mathbf{k}}$ on Fermi surfaces, (a) and (c) for PBE, (b) and (d) for OptB88-vdW functional, respectively. The red radii of circles in (a) and (b) indicate magnitude of EPC constant $\lambda_{\mathbf{q}v}$ at wave vector $\mathbf{q}$ and branch v. B1, B2, and B3 refer to the three bands crossing the Fermi level. Fermi surfaces are drawn by using the FERMISURFER code [54]. (c) and (d) have the same color scales. The first Brillouin zone of MgB_2 bulk is shown in B1 of (c).

Grimme's DFT-D2 [46] vdW correction are used. A real-space grid density that is equivalent to a plane-wave kinetic energy cutoff of 60 Ha is adopted. A 12 × 12 × 300 Monkhorst-Pack k-points mesh is set for the Brillouin-zone sampling of the surface structures. The topological indices [47,48] are obtained from a postprocessing procedure of the self-consistent calculations by ATK including the spin-orbital coupling interactions.

III. RESULTS AND DISCUSSION

Extensive efforts [4,18,49,50] have been made to theoretically reproduce the experimental T_c of an anisotropic superconductor such as MgB_2 [27]. The best T_c of MgB_2 obtained from SCDFT calculations was recently reported to be 35.4 K, based on the new functionals of electron-phonon superconducting pair interactions and electron-phonon renormalization factor [18]. This result is rather close to the experimental value [27]. As a benchmark, we reevaluate the superconductivities of MgB_2 again by using different exchange-correlation functionals from PBE [25,28], revPBE [29], and PBEsol [30] to OptB88-vdW [31–33]. The OPT functional includes the vdW dispersion force, which is essential to provide accurate predictions for structures of vdW layered materials [34,35,51].

Several key superconducting parameters of MgB_2 with either the experimental structure [27] or the optimized structure obtained with these functionals are shown in Tables I and SI in the Supplemental Material (SM) [52], respectively. Noticeably, the calculated T_c of MgB_2 is 39.3 K with the OptB88-vdW functional, in excellent agreement with the experimental value (39 K) [27]. It is worth noting that this is the best theoretical T_c of MgB_2 so far. In contrast, the PBE-based functionals seriously underestimate the T_c of MgB_2 for both cases without (T_c) and with ($T_{c\text{-SF}}$) SF.

The present results strongly suggest that the inclusion of the vdW correction is crucial in studies of MgB_2-type superconductors. This can be attributed to the fact that the OPT functional makes a slight downward shift of bands (see Fig. 1) and increases the density of states (DOS) at the Fermi level (D_0). The EPC constant λ (i.e., $\lambda_{\mathbf{q}v}$ and $\lambda_{n\mathbf{k}}$) thus increases (see Fig. 2) since it is proportional to D_0 [9]. The EPC is very strong near the Γ point and along the Γ-A path. The phonons obtained using the OPT functional are overall softened, especially for the bond-stretching mode (i.e., the E_{2g} mode) along the Γ-A path [53]. A large λ is observed due to the contributions of long-range interactions. The OPT functional appears to be more accurate in describing the electron-phonon interactions of MgB_2. It gives a larger electron-phonon renormalization factor Z_{ave} (average over the Fermi surface) than those from PBE functionals. This results in wider superconducting gaps whose maximum (Δ_{max}) and minimum (Δ_{min}) values are 9.63 and 1.18 meV, respectively (see Table I). Note that Fermi surfaces are drawn by using the FERMISURFER code [54].

The Coulomb pseudopotential μ^*_{ave} (average over the Fermi surface), which is usually treated as an adjustable parameter for the conventional Allen-Dynes-modified McMillan

TABLE II. Superconducting parameters of MgB_2 under different stretch strains (negative pressure).

Stretch strains (Kbar)	**a** (Å)	**c** (Å)	T_c (K)	Z_{ave}	Δ_{max} (meV)	Δ_{min} (meV)	λ_{ave}	μ^*_{ave}
0	3.034	3.470	29.4	0.64	7.08	0.91	0.68	0.28
50	3.062	3.538	35.6	0.72	8.71	1.06	0.77	0.28
75	3.079	3.577	40.3	0.79	9.83	1.23	0.83	0.28
100	3.096	3.621	45.1	0.87	11.20	1.34	0.92	0.28
110	3.104	3.640	48.9	0.91	11.86	1.44	0.96	0.28
125 (unstable)	3.116	3.671	53.3	0.99	12.99	1.65	1.05	0.28

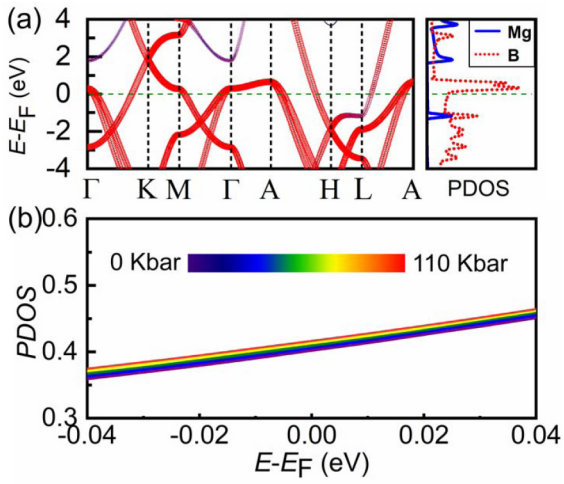

FIG. 3. (a) Projected band structures and projected density of states (PDOS) of MgB_2. (b) PDOS of B atom of MgB_2 under different stretch strains.

formula [9–11]:

$$T_c = \frac{\omega_{\ln}}{1.2} \exp\left[\frac{-1.04(1+\lambda)}{\lambda - \mu^*(1+0.62\lambda)}\right], \tag{4}$$

can be obtained via converse calculations of EPC constant λ and averaged phonon frequencies $\omega_{\ln}$, namely,

$$\lambda = \sum_{\mathbf{q}v} \lambda_{\mathbf{q}v}, \tag{5}$$

$$\lambda_{\mathbf{q}v} = \frac{2}{D_0 \omega_{\mathbf{q}v}} \sum_{\mathbf{k}nn'} \left| g^v_{n\mathbf{k}n'\mathbf{k}+\mathbf{q}} \right|^2 \delta(\xi_{n\mathbf{k}}) \delta(\xi_{n'\mathbf{k}+\mathbf{q}}), \tag{6}$$

$$\omega_{\ln} = \exp\left[\frac{1}{\lambda} \sum_{\mathbf{q}v} \lambda_{\mathbf{q}v} \ln(\omega_{\mathbf{q}v})\right], \tag{7}$$

where $\lambda_{\mathbf{q}v}$ and $\omega_{\mathbf{q}v}$ refer to the EPC constant and phonon frequency at wave vector $\mathbf{q}$ and branch v, respectively. Here, D_0 is the DOS at the E_F, and g is the electron-phonon matrix element [41]. The Brillouin-zone integrals are calculated using the optimized tetrahedron method [40] with a dense $\mathbf{k}$ grid. Although the EPC constant λ_{ave} (average over the Fermi surface) obtained with the OPT functional is the highest, these functionals produce the same Coulomb pseudopotential ($\mu^*_{\text{ave}} = 0.28$) that is much larger than the empirical value 0.10–0.16 [11].

Various methods have been attempted to increase T_c of superconductors, including high pressure [55,56], stretching [57], doping [58], and magic angle [59]. Most of these methods cause structural changes (e.g., lattice parameters). Note that the optimized structures are smaller than experimental ones and indeed give much reduced T_c for all functionals (see Table SI in the SM [52]), e.g., from 39.3 to 29.4 K for the OPT functional. In contrast, lattice stretch may significantly increase T_c of MgB_2 to a maximum value of 48.9 K (see Table II) under a strain of 110 Kbar (i.e., negative pressure). This is due to the enhanced PDOS value of B $2p$ orbitals near the E_F, which dominates the superconducting behavior of MgB_2 (see Fig. 3). We see that the Z_{ave}, $\Delta_{\max}$, $\Delta_{\min}$, and λ_{ave} of MgB_2 increase monotonically with the stretch, but

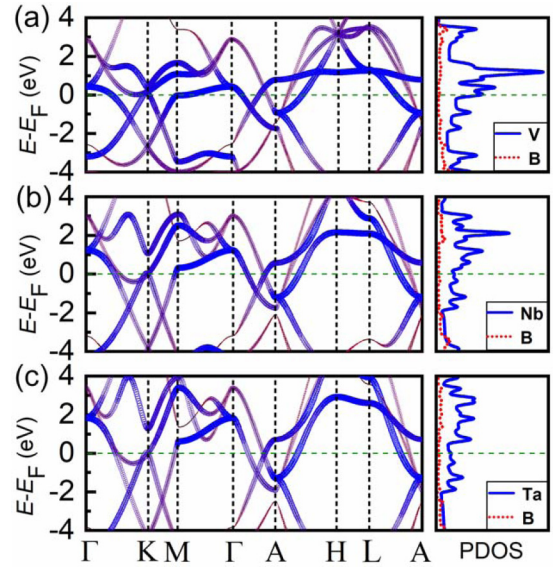

FIG. 4. Projected band structures and projected density of states (PDOS) of (a) VB_2, (b) NbB_2, and (c) TaB_2. The E_F is shifted to zero.

μ^*_{ave} remains unchanged (see Table II). Note that the MgB_2 remains stable under a reasonable stretch (<110 Kbar). Negative frequencies appear in phonon bands as the stretch is too large (such as 125 Kar in Fig. S1 in the SM [52]). Its lattice parameters (**a** and **c**) and T_c increase monotonically with the stretch (see Table II). Obviously, the appropriate geometry is one of the key factors for the reliable prediction of T_c. Furthermore, one may significantly enhance T_c of MgB_2 by applying a tensile strain.

We can now apply the same approach to study other transition metal diborides MB_2 (such as M = V, Nb, Ta). We first examine their electronic structures (see Fig. 4) and compare them with MgB_2. Their projected band structures are significantly different from that of MgB_2, and their states around E_F are mostly from transition metal elements rather than from B, as in MgB_2 (see Fig. 3). From results in Table III, VB_2 has a very low T_c (without SF) or $T_{c\text{-SF}}$ (with SF), <1 K, consistent with recent experimental obser-

TABLE III. Lattice parameters and superconductivities of VB-group MB_2 (M = V, Nb, Ta).

	VB_2	NbB_2	TaB_2
a (Å)	2.966	3.088	3.025
c (Å)	3.005	3.305	3.254
T_c (K)	0.97	10.2	13.8
$T_{c\text{-SF}}$ (K)	0.78[a]	7.9[b]	12.4[c]
$Z_{\text{ave-SF}}$	0.47	0.70	0.95
$\Delta_{\text{max-SF}}$ (meV)	0.27	2.33	3.08
$\Delta_{\text{min-SF}}$ (meV)	−0.39	0.38	1.06
λ_{ave}	0.30	0.68	0.92
$\mu^*_{\text{ave-SF}}$	0.66	0.31	0.25

[a]VB_2 is not superconducting beyond 2 K in experiment [60].
[b]The experimental T_c of NbB_2 are 9 K [64], 5 K [62], and 9.4 K [61].
[c]The experimental T_c of TaB_2 is 9.5 K [63].

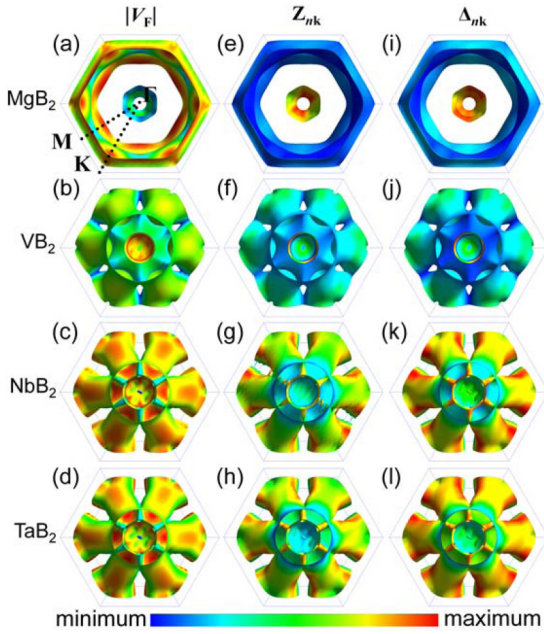

FIG. 5. Top views of Fermi velocity of the electronic states $|V_F|$, electron-phonon coupling renormalization $Z_{n\mathbf{k}}$, and superconducting gap function $\Delta_{n\mathbf{k}}$ on the cylindrical and "flying saucer"-like Fermi surfaces of (a) MgB_2, (b) VB_2, (c) NbB_2, and (d) $Ta\,B_2$. Their side views are shown in Fig. S2 of the Supplemental Material (SM) [52]. (a)–(d) for $|V_F|$, (e)–(h) for $Z_{n\mathbf{k}}$, and (i)–(l) for $\Delta_{n\mathbf{k}}$. The color bar indicates their minimum and maximum values.

vation [60]. Due to larger electron-phonon renormalization factor $Z_{\text{ave-SF}}$ and superconducting gap, NbB_2 and $Ta\,B_2$ have higher critical temperatures $T_{c\text{-SF}} = 7.9$ and 12.4 K. These values are closer to the corresponding experimental values [61–64] than those without considering SF. This demonstrates that SF plays a significant role in determining superconductivities of transition metal diborides. Note that the EPC constant λ_{ave} increases from VB_2 to NbB_2 and $Ta\,B_2$, but their Coulomb pseudopotential $\mu^*_{\text{ave-SF}}$ (see $\mu_{n\mathbf{k}}$ in Fig. S3 in the SM [52]) shows a reverse trend. This is associated with the softened acoustic vibrations arising from the change of mass of transition metal atoms (see Fig. S4 in the SM [52]).

To gain deeper insights into the superconducting behaviors of these diborides, we depict the Fermi velocities $|V_F|$ of the normal electronic states, electron-phonon renormalization factor $Z_{n\mathbf{k}}$, and superconducting gap $\Delta_{n\mathbf{k}}$ on Fermi surfaces in Fig. 5.On first glance, $|V_F|$, $Z_{n\mathbf{k}}$, and $\Delta_{n\mathbf{k}}$ of these materials are very anisotropic. For instance, the ratio between the maximum and the minimum values of $|V_F|$ for $Ta\,B_2$ is as high as 213. For MgB_2, there are three bands crossing E_F, and its $|V_F|$ is mostly dominated by the B $2p$ orbitals, especially on the cylindrical Fermi surfaces around the Γ point [see Fig. 5(a)]. This contributes the most of $Z_{n\mathbf{k}}$ [see Fig. 5(e)] and $\Delta_{n\mathbf{k}}$ [see Fig. 5(i)]. The Fermi surfaces of MB_2 appear like a "flying saucer" with a large cavity around the Γ point (see the top views in Fig. 5 and side views in Fig. S2 in the SM [52]). Although MB_2 diborides have four bands crossing E_F (except VB_2 which has three), the crossing points are far from the Γ point. Their $|V_F|$ are typically small, as these states are mostly from localized transition metal orbitals. The magnitudes of their $|V_F|$, $Z_{n\mathbf{k}}$, and $\Delta_{n\mathbf{k}}$ increase from VB_2 to NbB_2 and $Ta\,B_2$, leading to gradual increase of T_c.

It is found that the ratio of DOS at the E_F between B and metal atoms gradually increases from VB_2 (1:6.6) to NbB_2 (1:3.2) and $Ta\,B_2$ (1:2.5) but remains much smaller than that of MgB_2 (295.7:1). As a result, their T_c follow the trend of $T_c(VB_2) < T_c(NbB_2) < T_c(Ta\,B_2) < T_c(MgB_2)$. This suggests that the T_c of VB-group diborides can be further enhanced if one may increase the PDOS of the B atom, such as by applying a lattice stretch that can lead to the increase of $Z_{\text{ave-SF}}$, $\Delta_{\text{max-SF}}$, $\Delta_{\text{min-SF}}$, and λ_{ave}. Table IV shows the results of $Ta\,B_2$ under different tensile strains. It can be observed that, as its lattice parameters **a** and **c** increase, T_c can be enhanced to 16.1 K at a negative pressure of 150 Kbar, under which the $Ta\,B_2$ is still stable without any negative frequency phonon branch (see Fig. S5 in the SM [52]).

The topological state of quantum materials has drawn tremendous attention in recent years. It is also interesting to further examine the topological properties of these VB-group diborides such as $Ta\,B_2$ and NbB_2 which have high T_c. From the experimental perspective, the angle-resolved photoemission spectroscopy (ARPES) represents a powerful tool in probing the electronic structures, superconductivity, and topological properties of materials [65]. Theoretically, the topology denoted by topological indices $Z_2(\nu_0; \nu_1\ \nu_2\ \nu_3)$ can be determined by the symmetry of Bloch functions at eight special time-reversal invariant points, including one strong topological index ν_0 and three weak indices ν_1, ν_2, ν_3 [47,48,66,67]. It is found that both $Ta\,B_2$ and NbB_2 are characterized by weak Z_2 indices (0;001). This is the same as MgB_2, whose topological surface states were observed in recent experiments [68]. Our result is consistent with a recent theoretical report [66].

To further check the topological status of VB-group diborides, we construct the $Ta\,B_2$ and NbB_2 (001) surfaces [see Fig. 6(a)] and study their surface states using the Green's function approach [69,70]. Using the Green's function surface model [71], the work function (Φ) of $Ta\,B_2$ and NbB_2 (001)

TABLE IV. Superconducting parameters of $Ta\,B_2$ under different stretch strains.

Stretch strains (Kbar)	**a** (Å)	**c** (Å)	$T_{c\text{-SF}}$ (K)	$Z_{\text{ave-SF}}$	$\Delta_{\text{max-SF}}$ (meV)	$\Delta_{\text{min-SF}}$ (meV)	λ_{ave}	$\mu^*_{\text{ave-SF}}$
0	3.025	3.254	12.4	0.95	3.08	1.06	0.92	0.25
75	3.048	3.289	13.9	1.07	3.45	1.25	1.03	0.25
100	3.056	3.302	14.6	1.12	3.59	1.32	1.08	0.26
125	3.065	3.315	15.2	1.18	3.74	1.41	1.13	0.26
150	3.074	3.329	16.1	1.25	3.72	1.50	1.20	0.26

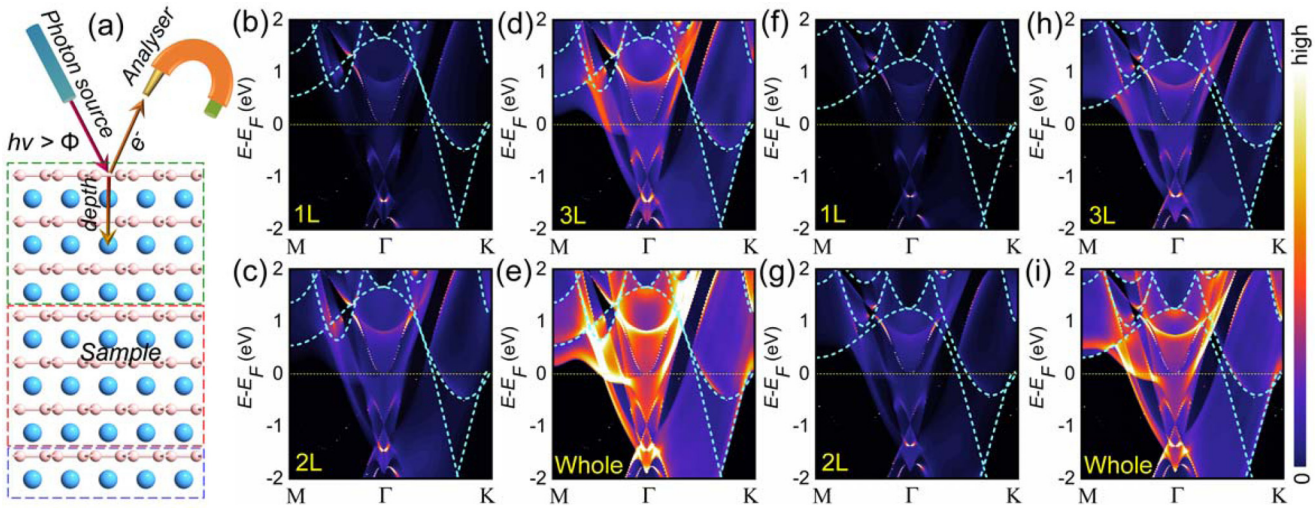

FIG. 6. (a) Schematic of detecting the electronic structures of MB_2 surface by angle-resolved photoemission spectroscopy (ARPES) set. The photon source energy $h\nu$ should be larger than the work function Φ of MB_2. The blue, red, and green dotted lines refer to the semi-infinite bulk, screening layers, and surface region of the used surface model, respectively. Spectral function with detection depths to the outermost monolayer (1L), the second layer (2L), the third layer (3L), as well as the whole slab structure (Whole). (b)–(e) for $Ta\,B_2$ surface, (f)–(i) for NbB_2 surface. The sky blue dotted lines in (b)–(i) indicate the band structures of $Ta\,B_2$ and NbB_2 bulk.

surfaces are 6.21 and 6.30 eV, respectively. To compare with ARPES, the spectral function is determined as

$$A(E, \mathbf{k}_{||}) = -\frac{1}{\pi}\mathrm{Im}[\mathbf{G}_{\mathbf{k}_{||}}(E)], \tag{8}$$

$$\mathbf{G}_{\mathbf{k}_{||}}(E) = \left[E - \mathbf{H}^{\mathrm{DFT}}_{\mathrm{K}_{||}} - \mathbf{\Sigma}_{\mathrm{K}_{||}}(E)\right]^{-1}. \tag{9}$$

Here, $\mathbf{k}_{||} = (k_a, k_b)$ is the transverse k-vector, $\mathbf{G}_{\mathbf{k}_{||}}(E)$ is the retarded Green's function of the surface system, $\mathbf{H}^{\mathrm{DFT}}_{\mathrm{K}_{||}}$ refers to the DFT Hamiltonian of the surface region and the screening layers, and $\mathbf{\Sigma}_{\mathrm{K}_{||}}(E)$ is the self-energy of the semi-infinite bulk part.

In ARPES measurements, the detector may display different features, depending on the probing depth. Figures 6(b)–6(e) give the spectral functions with detection depths to the outermost $Ta\,B_2$ monolayer (labeled 1L), the second layer (2L), the third layer (3L), and the whole slab (Whole) of the $Ta\,B_2$ (001) surface, respectively. We see that the 1L spectral function clearly illustrates the topological surface phase with a robust Dirac state near E_F around the Γ point. Its topological surface states become stronger when the detection depth increases. Figures 6(f)–6(i) illustrate the spectral functions of the NbB_2 (111) surface with different probing depths, where the same topological nature can be observed as $Ta\,B_2$. These results imply that both $Ta\,B_2$ and NbB_2 have potential applications for integrating superconductivity and topological properties in a single system.

IV. CONCLUSIONS

In conclusion, we have investigated the superconductivities and topological properties of several MgB_2-type vdW layered structures using different exchange-correlation functionals. DFT for superconductors can accurately reproduce T_c of MgB_2 when the OptB88-vdW functional is adopted. The spin fluctuation was found to play a significant role in the superconductivities of VB-group diborides. In addition, we found that their T_c can be further enhanced by applying reasonable stretch strains. This paper explicitly draws attention to the following key factors when one simulates superconductivities of materials, i.e., the reliable geometry, proper exchange-correlation functional such as those with the vdW correction, and inclusion of key mechanisms, such as the spin-fluctuation for real materials. Moreover, we demonstrated that both $Ta\,B_2$ and NbB_2 have a topological surface state, suggesting their potential utilizations as topological superconductors in quantum devices. This paper may stimulate further development for the prediction of superconductors, with or without the topological properties.

ACKNOWLEDGMENTS

Work in China was supported by the National Natural Science Foundation of China (Grants No. 11774079 and No. 61774059), the Scientific and Technological Innovation Program of Henan Province's Universities (Grant No. 20HASTIT026), the Natural Science Foundation of Henan Province (No. 202300410226), the Young Top-notch Talents Project of Henan Province (2021 year), the Natural Science Foundation of Henan Normal University (No. 2020PL15), the Henan Overseas Expertise Introduction Center for Discipline Innovation (No. CXJD2019005), and the HPCC of HNU. Work at the UC Irvine was supported by the U.S. Department of Energy, Basic Energy Science (Grant No. DE-FG02-05ER46237). We thank J. P. Hu at IOP of CAS for helpful discussions.

[1] J. Bardeen, L. N. Cooper, and J. R. Schrieffer, Phys. Rev. **108**, 1175 (1957).
[2] G. M. Eliashberg, J. Exp. Theor. Phys. **38**, 966 (1960) [Sov. Phys. JETP **11**, 696 (1960)].
[3] A. B. Migdal, J. Exp. Theor. Phys. **34**, 1438 (1958) [Sov. Phys. JETP **7**, 996 (1958)].
[4] E. R. Margine and F. Giustino, Phys. Rev. B **87**, 024505 (2013).
[5] C.-S. Lian, C. Si, and W. Duan, Nano Lett. **18**, 2924 (2018).
[6] Y. Zhao, C. Lian, S. Zeng, Z. Dai, S. Meng, and J. Ni, Phys. Rev. B **101**, 104507 (2020).
[7] L. Yan, P.-F. Liu, H. Li, Y. Tang, J. He, X. Huang, B.-T. Wang, and L. Zhou, npj Comput. Mater. **6**, 94 (2020).
[8] P. Morel and P. W. Anderson, Phys. Rev. **125**, 1263 (1962).
[9] W. L. McMillan, Phys. Rev. **167**, 331 (1968).
[10] R. C. Dynes, Solid State Commun. **10**, 615 (1972).
[11] P. B. Allen and R. C. Dynes, Phys. Rev. B **12**, 905 (1975).
[12] J. A. Flores-Livas, L. Boeri, A. Sanna, G. Profeta, R. Arita, and M. Eremets, Phys. Rep. **856**, 1 (2020).
[13] L. N. Oliveira, E. K. U. Gross, and W. Kohn, Phys. Rev. Lett. **60**, 2430 (1988).
[14] M. Lüders, M. A. L. Marques, N. N. Lathiotakis, A. Floris, G. Profeta, L. Fast, A. Continenza, S. Massidda, and E. K. U. Gross, Phys. Rev. B **72**, 024545 (2005).
[15] M. A. L. Marques, M. Lüders, N. N. Lathiotakis, G. Profeta, A. Floris, L. Fast, A. Continenza, E. K. U. Gross, and S. Massidda, Phys. Rev. B **72**, 024546 (2005).
[16] J. A. Flores-Livas and A. Sanna, Phys. Rev. B **91**, 054508 (2015).
[17] M. Kawamura, R. Akashi, and S. Tsuneyuki, Phys. Rev. B **95**, 054506 (2017).
[18] A. Sanna, C. Pellegrini, and E. K. U. Gross, Phys. Rev. Lett. **125**, 057001 (2020).
[19] M. Kawamura, Y. Hizume, and T. Ozaki, Phys. Rev. B **101**, 134511 (2020).
[20] J. A. Flores-Livas, A. Sanna, and E. K. U. Gross, Eur. Phys. J. B **89**, 63 (2016).
[21] R. Akashi and R. Arita, Phys. Rev. Lett. **111**, 057006 (2013).
[22] F. Essenberger, A. Sanna, A. Linscheid, F. Tandetzky, G. Profeta, P. Cudazzo, and E. K. U. Gross, Phys. Rev. B **90**, 214504 (2014).
[23] T. Nomoto, M. Kawamura, T. Koretsune, R. Arita, T. Machida, T. Hanaguri, M. Kriener, Y. Taguchi, and Y. Tokura, Phys. Rev. B **101**, 014505 (2020).
[24] A. Floris, A. Sanna, M. Lüders, G. Profeta, N. N. Lathiotakis, M. A. L. Marques, C. Franchini, E. K. U. Gross, A. Continenza, and S. Massidda, Phys. C: Supercond. **456**, 45 (2007).
[25] J. P. Perdew, K. Burke, and M. Ernzerhof, Phys. Rev. Lett. **77**, 3865 (1996).
[26] D. Vanderbilt, Phys. Rev. B **41**, 7892 (1990).
[27] J. Nagamatsu, N. Nakagawa, T. Muranaka, Y. Zenitani, and J. Akimitsu, Nature (London) **410**, 63 (2001).
[28] J. P. Perdew, J. A. Chevary, S. H. Vosko, K. A. Jackson, M. R. Pederson, D. J. Singh, and C. Fiolhais, Phys. Rev. B **46**, 6671 (1992).
[29] Y. Zhang and W. Yang, Phys. Rev. Lett. **80**, 890 (1998).
[30] J. P. Perdew, A. Ruzsinszky, G. I. Csonka, O. A. Vydrov, G. E. Scuseria, L. A. Constantin, X. Zhou, and K. Burke, Phys. Rev. Lett. **100**, 136406 (2008).
[31] J. Klimeš, D. R. Bowler, and A. Michaelides, J. Phys.: Condens. Matter **22**, 022201 (2009).
[32] T. Thonhauser, S. Zuluaga, C. A. Arter, K. Berland, E. Schröder, and P. Hyldgaard, Phys. Rev. Lett. **115**, 136402 (2015).
[33] T. Thonhauser, V. R. Cooper, S. Li, A. Puzder, P. Hyldgaard, and D. C. Langreth, Phys. Rev. B **76**, 125112 (2007).
[34] K. Choudhary, G. Cheon, E. Reed, and F. Tavazza, Phys. Rev. B **98**, 014107 (2018).
[35] K. Choudhary, K. F. Garrity, A. C. E. Reid, B. DeCost, A. J. Biacchi, A. R. Hight Walker, Z. Trautt, J. Hattrick-Simpers, A. Gilad Kusne, A. Centrone *et al.*, npj Comput. Mater. **6**, 173 (2020).
[36] P. Giannozzi, O. Andreussi, T. Brumme, O. Bunau, M. Buongiorno Nardelli, M. Calandra, R. Car, C. Cavazzoni, D. Ceresoli, M. Cococcioni *et al.*, J. Phys.: Condens. Matter **29**, 465901 (2017).
[37] D. R. Hamann, Phys. Rev. B **88**, 085117 (2013).
[38] M. Schlipf and F. Gygi, Comput. Phys. Commun. **196**, 36 (2015).
[39] G. Prandini, A. Marrazzo, I. E. Castelli, N. Mounet, and N. Marzari, npj Comput. Mater. **4**, 72 (2018).
[40] M. Kawamura, Y. Gohda, and S. Tsuneyuki, Phys. Rev. B **89**, 094515 (2014).
[41] S. Baroni, S. de Gironcoli, A. Dal Corso, and P. Giannozzi, Rev. Mod. Phys. **73**, 515 (2001).
[42] http://sctk.osdn.jp/.
[43] J. Taylor, H. Guo, and J. Wang, Phys. Rev. B **63**, 121104(R) (2001).
[44] M. Brandbyge, J.-L. Mozos, P. Ordejón, J. Taylor, and K. Stokbro, Phys. Rev. B **65**, 165401 (2002).
[45] J. M. Soler, E. Artacho, J. D. Gale, A. García, J. Junquera, P. Ordejón, and D. Sánchez-Portal, J. Phys.: Condens. Matter **14**, 2745 (2002).
[46] S. Grimme, J. Comput. Chem. **27**, 1787 (2006).
[47] L. Fu and C. L. Kane, Phys. Rev. B **76**, 045302 (2007).
[48] L. Fu, C. L. Kane, and E. J. Mele, Phys. Rev. Lett. **98**, 106803 (2007).
[49] H. J. Choi, D. Roundy, H. Sun, M. L. Cohen, and S. G. Louie, Nature (London) **418**, 758 (2002).
[50] A. Floris, G. Profeta, N. N. Lathiotakis, M. Lüders, M. A. L. Marques, C. Franchini, E. K. U. Gross, A. Continenza, and S. Massidda, Phys. Rev. Lett. **94**, 037004 (2005).
[51] D. Yuan, Y. Zhang, W. Ho, and R. Wu, J. Phys. Chem. C **124**, 16926 (2020).
[52] See Supplemental Material at http://link.aps.org/supplemental/10.1103/PhysRevB.104.134510 for more details of partial results, which includes Refs. [11,27,47,48,55–57].
[53] A. Shukla, M. Calandra, M. d'Astuto, M. Lazzeri, F. Mauri, C. Bellin, M. Krisch, J. Karpinski, S. M. Kazakov, J. Jun, D. Daghero, and K. Parlinski, Phys. Rev. Lett. **90**, 095506 (2003).
[54] M. Kawamura, Comput. Phys. Commun. **239**, 197 (2019).
[55] I. Errea, F. Belli, L. Monacelli, A. Sanna, T. Koretsune, T. Tadano, R. Bianco, M. Calandra, R. Arita, F. Mauri, and J. A. Flores-Livas, Nature (London) **578**, 66 (2020).
[56] X.-M. Zhao, K. Zhang, Z.-Y. Cao, Z.-W. Zhao, V. V. Struzhkin, A. F. Goncharov, H.-K. Wang, A. G. Gavriliuk, H.-K. Mao, and X.-J. Chen, Phys. Rev. B **101**, 134506 (2020).
[57] X. Zhang, M. Zhao, and F. Liu, Phys. Rev. B **100**, 104527 (2019).
[58] J.-J. Zheng and E. R. Margine, Phys. Rev. B **94**, 064509 (2016).

[59] Y. Cao, V. Fatemi, S. Fang, K. Watanabe, T. Taniguchi, E. Kaxiras, and P. Jarillo-Herrero, Nature (London) **556**, 43 (2018).

[60] P. Wang, R. Kumar, E. M. Sankaran, X. Qi, X. Zhang, D. Popov, A. L. Cornelius, B. Li, Y. Zhao, and L. Wang, Inorg. Chem. **57**, 1096 (2018).

[61] J. E. Schirber, D. L. Overmyer, B. Morosin, E. L. Venturini, R. Baughman, D. Emin, H. Klesnar, and T. Aselage, Phys. Rev. B **45**, 10787 (1992).

[62] H. Kotegawa, K. Ishida, Y. Kitaoka, T. Muranaka, N. Nakagawa, H. Takagiwa, and J. Akimitsu, Phys. C: Supercond. **378–381**, 25 (2002).

[63] D. Kaczorowski, A. J. Zaleski, O. J. Żogał, and K. Klamut, arXiv:cond-mat/0103571.

[64] H. Takeya, K. Togano, Y. S. Sung, T. Mochiku, and K. Hirata, Phys. C: Supercond. **408–410**, 144 (2004).

[65] C. Li, X. Wu, L. Wang, D. Liu, Y. Cai, Y. Wang, Q. Gao, C. Song, J. Huang, C. Dong *et al.*, Phys. Rev. X **10**, 031033 (2020).

[66] K.-H. Jin, H. Huang, J.-W. Mei, Z. Liu, L.-K. Lim, and F. Liu, npj Comput. Mater. **5**, 57 (2019).

[67] Y. Zhou, B. Li, Z. Lou, H. Chen, Q. Chen, B. Xu, C. Wu, J. Du, J. Yang, H. Wang, and M. Fang, Sci. China Phys. Mech. Astron. **64**, 247411 (2021).

[68] X. Zhou, K. N. Gordon, K.-H. Jin, H. Li, D. Narayan, H. Zhao, H. Zheng, H. Huang, G. Cao, N. D. Zhigadlo, F. Liu, and D. S. Dessau, Phys. Rev. B **100**, 184511 (2019).

[69] J. M. Marmolejo-Tejada, K. Dolui, P. Lazić, P.-H. Chang, S. Smidstrup, D. Stradi, K. Stokbro, and B. K. Nikolić, Nano Lett. **17**, 5626 (2017).

[70] S. Smidstrup, D. Stradi, J. Wellendorff, P. A. Khomyakov, U. G. Vej-Hansen, M.-E. Lee, T. Ghosh, E. Jónsson, H. Jónsson, and K. Stokbro, Phys. Rev. B **96**, 195309 (2017).

[71] Y. An, Y. Hou, S. Gong, R. Wu, C. Zhao, T. Wang, Z. Jiao, H. Wang, and W. Liu, Phys. Rev. B **101**, 075416 (2020).